PHYSICAL REVIEW D **96,** 016006 (2017)

$SU(3)$ sphaleron: Numerical solution

F. R. Klinkhamer* and P. Nagel†

Institute for Theoretical Physics, Karlsruhe Institute of Technology (KIT), 76128 Karlsruhe, Germany

(Received 3 May 2017; published 12 July 2017)

We complete the construction of the sphaleron $\hat{S}$ in $SU(3)$ Yang-Mills-Higgs theory with a single Higgs triplet by solving the reduced field equations numerically. The energy of the $SU(3)$ sphaleron $\hat{S}$ is found to be of the same order as the energy of a previously known solution, the embedded $SU(2) \times U(1)$ sphaleron S. In addition, we discuss $\hat{S}$ in an extended $SU(3)$ Yang-Mills-Higgs theory with three Higgs triplets, where all eight gauge bosons get an equal mass in the vacuum. This extended $SU(3)$ Yang-Mills-Higgs theory may be considered as a toy model of quantum chromodynamics without quark fields and we conjecture that the $\hat{S}$ gauge fields play a significant role in the nonperturbative dynamics of quantum chromodynamics (which does not have fundamental scalar fields but gets a mass scale from quantum effects).

DOI: 10.1103/PhysRevD.96.016006

I. INTRODUCTION

The non-Abelian chiral gauge anomaly [1] is expected to be associated [2] with a new type of sphaleron (a static, but unstable, finite-energy solution of the classical field equations). A self-consistent *Ansatz* for this sphaleron, denoted $\hat{S}$, has indeed been constructed in $SU(3)$ Yang–Mills–Higgs theory [3]. But the numerical solution of the reduced field equations and the corresponding determination of the energy $E_{\hat{S}}$ have turned out to be challenging. In this article, we present, at last, the numerical solution of the $\hat{S}$ fields in the basic $SU(3)$ Yang–Mills–Higgs theory with a single Higgs triplet and find a surprisingly low value of the energy $E_{\hat{S}}$, namely an energy of the same order as (and even below) the energy E_S of the embedded $SU(2) \times U(1)$ sphaleron S [4–6].

The outline of the present article is as follows. In Sec. II, we define two classical $SU(3)$ Yang–Mills–Higgs theories. The first theory has a single Higgs triplet and the second theory has three Higgs triplets (designed to give an equal mass to all eight gauge bosons in the vacuum). The focus of the main part of this article will be on the basic $SU(3)$ Yang–Mills–Higgs theory with a single Higgs triplet. In Sec. III, we give a brief sketch of the topological argument (minimax procedure) and recall the $\hat{S}$ *Ansatz* from Ref. [3]. In Sec. IV, we consider the reduced field equations and solve them analytically near the origin. In Sec. V, we present the numerical solution obtained by a minimization procedure of the *Ansatz* energy. In Sec. VI, we give the corresponding results for $\hat{S}$ in the extended $SU(3)$ Yang–Mills–Higgs theory with three Higgs triplets. In Sec. VII, we present concluding remarks.

There are also five appendices with technical details. For the basic $SU(3)$ Yang–Mills–Higgs theory, Appendix A gives the $\hat{S}$ energy density and Appendix B presents the expansion coefficients for the $\hat{S}$ *Ansatz* functions. For the extended $SU(3)$ Yang–Mills–Higgs theory, Appendix C presents the noncontractible sphere of configurations needed for the $\hat{S}$ *Ansatz*, Appendix D gives the $\hat{S}$ energy density, and Appendix E discusses the minimization setup.

II. TWO $SU(3)$ YANG–MILLS–HIGGS THEORIES

We consider two classical $SU(3)$ Yang–Mills–Higgs (YMH) theories. The first theory is a direct enlargement [7] of the $SU(2) \times U(1)$ electroweak Standard Model with weak mixing angle $\theta_w = \pi/6$. The second theory may be considered as a toy model of a simplified version of quantum chromodynamics (QCD) [8] without quark fields, having eight gauge bosons of equal mass (taken to model the quantum effects of QCD). Some further remarks on the possible relevance of the second $SU(3)$ YMH theory for quarkless QCD are presented in Sec. VI D. The first $SU(3)$ Yang–Mills–Higgs theory is the one used in the original $\hat{S}$ paper [3] and will be the main focus of the present article.

A. Basic $SU(3)$ YMH theory

The first $SU(3)$ Yang–Mills–Higgs theory considered has a single triplet Φ of complex scalar fields. The classical action is given by

$$S = \int_{\mathbb{R}^4} d^4x \left\{ \frac{1}{2}\mathrm{tr} F_{\mu\nu} F^{\mu\nu} + (D_\mu \Phi)^\dagger (D^\mu \Phi) - \lambda(\Phi^\dagger \Phi - \eta^2)^2 \right\}, \tag{2.1}$$

where $F_{\mu\nu} \equiv \partial_\mu A_\nu - \partial_\nu A_\mu + g[A_\mu, A_\nu]$ is the $SU(3)$ Yang–Mills field strength tensor and $D_\mu \equiv (\partial_\mu + g A_\mu)$ the covariant derivative for the triplet representation of $SU(3)$. The Higgs field has a global $U(1)$ symmetry, $\Phi(x) \to e^{i\omega}\Phi(x)$.

*frans.klinkhamer@kit.edu
†pascal.nagel@kit.edu

The constant η is assumed to be nonzero and the standard electroweak notation is obtained by setting $\eta = v/\sqrt{2}$.

The $SU(3)$ Yang–Mills gauge field is defined as

$$A_\mu(x) \equiv A^a_\mu(x)\lambda_a/(2i), \tag{2.2}$$

in terms of the eight Gell-Mann matrices

$$\lambda_1 = \begin{pmatrix} 0 & 1 & 0 \\ 1 & 0 & 0 \\ 0 & 0 & 0 \end{pmatrix}, \quad \lambda_2 = \begin{pmatrix} 0 & -i & 0 \\ i & 0 & 0 \\ 0 & 0 & 0 \end{pmatrix},$$
$$\lambda_3 = \begin{pmatrix} 1 & 0 & 0 \\ 0 & -1 & 0 \\ 0 & 0 & 0 \end{pmatrix}, \quad \lambda_4 = \begin{pmatrix} 0 & 0 & 1 \\ 0 & 0 & 0 \\ 1 & 0 & 0 \end{pmatrix},$$
$$\lambda_5 = \begin{pmatrix} 0 & 0 & -i \\ 0 & 0 & 0 \\ i & 0 & 0 \end{pmatrix}, \quad \lambda_6 = \begin{pmatrix} 0 & 0 & 0 \\ 0 & 0 & 1 \\ 0 & 1 & 0 \end{pmatrix},$$
$$\lambda_7 = \begin{pmatrix} 0 & 0 & 0 \\ 0 & 0 & -i \\ 0 & i & 0 \end{pmatrix}, \quad \lambda_8 = \frac{1}{\sqrt{3}} \begin{pmatrix} 1 & 0 & 0 \\ 0 & 1 & 0 \\ 0 & 0 & -2 \end{pmatrix}. \tag{2.3}$$

The field $\Phi(x)$ is a triplet of complex scalar fields,

$$\Phi(x) = \begin{pmatrix} \Phi_1(x) \\ \Phi_2(x) \\ \Phi_3(x) \end{pmatrix}, \tag{2.4}$$

which acquires a vacuum expectation value η due to the Higgs potential term in the action (2.1). Throughout, we use the Minkowski spacetime metric $g_{\mu\nu}(x) = \eta_{\mu\nu} = [\text{diag}(+1, -1, -1, -1)]_{\mu\nu}$ and natural units with $\hbar = c = 1$.

The scalar vacuum field can be chosen as

$$\Phi = \begin{pmatrix} 0 \\ 0 \\ \eta \end{pmatrix}, \tag{2.5}$$

which gives a mass to five gauge fields, A^a_μ for $a = 4, 5, 6, 7, 8$, with three gauge fields remaining massless, A^a_μ for $a = 1, 2, 3$. There is one physical scalar mode $(3 \times 2 - 5 = 1)$, which is massive for a nonvanishing quartic Higgs coupling, $\lambda > 0$. Equivalent Higgs vacua can, for example, be obtained by transformation with the following $SU(3)$ matrices:

$$M_1 \equiv \begin{pmatrix} 1 & 0 & 0 \\ 0 & 0 & 1 \\ 0 & -1 & 0 \end{pmatrix}, \qquad M_2 \equiv \begin{pmatrix} 0 & 0 & 1 \\ 0 & 1 & 0 \\ -1 & 0 & 0 \end{pmatrix},$$
$$M_3 \equiv \begin{pmatrix} 0 & 1 & 0 \\ -1 & 0 & 0 \\ 0 & 0 & 1 \end{pmatrix}. \tag{2.6}$$

One such equivalent Higgs vacuum is

$$\Phi = M_2 \cdot \begin{pmatrix} 0 \\ 0 \\ \eta \end{pmatrix} = \begin{pmatrix} \eta \\ 0 \\ 0 \end{pmatrix}, \tag{2.7}$$

which will be used for the $\hat{S}$ *Ansatz* later on.

B. Extended $SU(3)$ YMH theory

The second $SU(3)$ Yang–Mills–Higgs theory considered has three triplets of complex scalar fields, Φ_α for $\alpha = 1, 2, 3$. The classical action is given by

$$\begin{aligned} S = \int_{\mathbb{R}^4} d^4x \Big\{ & \frac{1}{2}\text{tr} F_{\mu\nu} F^{\mu\nu} \\ & + \sum_{\alpha=1}^{3} [(D_\mu \Phi_\alpha)^\dagger (D^\mu \Phi_\alpha) - \lambda(\Phi^\dagger_\alpha \Phi_\alpha - \eta^2)^2] \\ & - \lambda(\Phi^\dagger_1 \Phi_2)(\Phi^\dagger_2 \Phi_1) - \lambda(\Phi^\dagger_1 \Phi_3)(\Phi^\dagger_3 \Phi_1) \\ & - \lambda(\Phi^\dagger_2 \Phi_3)(\Phi^\dagger_3 \Phi_2) \Big\}. \end{aligned} \tag{2.8}$$

The Higgs fields have a global $U(1) \times U(1) \times U(1)$ symmetry.

The scalar vacuum fields can be chosen as

$$\Phi_1 = \begin{pmatrix} \eta \\ 0 \\ 0 \end{pmatrix}, \qquad \Phi_2 = \begin{pmatrix} 0 \\ \eta \\ 0 \end{pmatrix}, \qquad \Phi_3 = \begin{pmatrix} 0 \\ 0 \\ \eta \end{pmatrix}, \tag{2.9}$$

which give an equal mass $(m_A = g\eta)$ to all eight gauge fields A^a_μ. There are ten physical scalar modes $(3 \times 3 \times 2 - 8 = 10)$, nine of which are massive for quartic Higgs coupling $\lambda > 0$ and one of which remains massless. This last massless mode can get a mass from a more complicated Higgs sector, but, in this paper, we keep the relatively simple extended $SU(3)$ YMH theory as given by (2.8).

III. $\hat{S}$ ANSATZ IN THE BASIC $SU(3)$ YMH THEORY

The logic behind the existence of the new sphaleron $\hat{S}$ in $SU(3)$ Yang–Mills–Higgs theory with a single Higgs triplet

and the derivation of the $\hat{S}$ *Ansatz* have been explained in Ref. [3], but will be briefly recalled below. For our present purpose, the focus will be on the *Ansatz* fields and the corresponding energy density. Both will be specialized to the radial gauge. Standard spherical polar coordinates (r, θ, ϕ) are used, defined, in terms of the Cartesian coordinates by $(x, y, z) = (r\sin\theta\cos\phi, r\sin\theta\sin\phi, r\cos\theta)$.

A. Minimax procedure

For completeness, we sketch how the *Ansatz* for $\hat{S}$ was obtained in Ref. [3]. The idea is to consider the mathematical space of finite-energy gauge and Higgs field configurations of the theory considered. A noncontractible 3-sphere can be constructed in this configuration space, where the 3-sphere is parameterized by spherical coordinates with polar angles ψ and μ and azimuthal angle α. One point V of that 3-sphere (at $\psi = 0$) corresponds to the configurations of the vacuum.

Next, evaluate the energy for all configurations of this noncontractible sphere (NCS). The point V (at $\psi = 0$) has energy $E = 0$ and the other points of the NCS have $E > 0$. The configuration at $\psi = \pi$ has extra discrete symmetries of the fields and is, generically, the one with the highest energy. The qualitative picture is that of a 3-sphere with the lowest-energy point at $\psi = 0$ and the highest-energy point at $\psi = \pi$.

We now follow a minimax procedure: the maximum configuration $(\psi = \pi)$ is minimized by improving the profile functions of the fields, in order to arrive at a genuine solution $(\hat{S})$ of the YMH field equations (which needs to be verified explicitly). The same minimax procedure for a noncontractible loop (1-sphere) has given the sphaleron S [4] and for a noncontractible 2-sphere has given the sphaleron S^* [9]; see Sec. IV of Ref. [10] for a review and further references.

Details of the NCS for $\hat{S}$ can be found in Ref. [3] and in Appendix C here, where the two extra Higgs triplets can be neglected for the NCS relevant to the basic $SU(3)$ YMH theory.

B. Gauge and Higgs field Ansätze

The $\hat{S}$ gauge fields in the radial gauge are given by [3]

$$g\hat{A}_0(r,\theta,\phi) = 0, \tag{3.1a}$$

$$g\hat{A}_\phi(r,\theta,\phi) = \alpha_1(r,\theta)\cos\theta T_\rho + \alpha_2(r,\theta)V_\rho + \alpha_3(r,\theta)\cos\theta U_\rho + \alpha_4(r,\theta)\frac{\lambda_3}{2i} + \alpha_5(r,\theta)\frac{\lambda_8}{2i}, \tag{3.1b}$$

$$g\hat{A}_\theta(r,\theta,\phi) = \alpha_6(r,\theta)T_\phi + \alpha_7(r,\theta)\cos\theta V_\phi + \alpha_8(r,\theta)U_\phi, \tag{3.1c}$$

$$g\hat{A}_r(r,\theta,\phi) = 0, \tag{3.1d}$$

with real functions $\alpha_i(r,\theta)$ that are required to have positive parity with respect to reflection of the z-coordinate,

$$\alpha_i(r,\pi-\theta) = +\alpha_i(r,\theta), \quad \text{for } i = 1,\ldots,8. \tag{3.2}$$

The gauge fields (3.1) involve the following generators of the $su(3)$ Lie algebra:

$$T_\phi \equiv -\sin\phi\frac{\lambda_1}{2i} + \cos\phi\frac{\lambda_2}{2i}, \qquad T_\rho \equiv \cos\phi\frac{\lambda_1}{2i} + \sin\phi\frac{\lambda_2}{2i}, \qquad T_3 \equiv \frac{\lambda_3}{2i}, \tag{3.3a}$$

$$V_\phi \equiv +\sin\phi\frac{\lambda_4}{2i} + \cos\phi\frac{\lambda_5}{2i}, \qquad V_\rho \equiv \cos\phi\frac{\lambda_4}{2i} - \sin\phi\frac{\lambda_5}{2i}, \qquad V_3 \equiv \frac{\sqrt{3}\lambda_8 + \lambda_3}{4i}, \tag{3.3b}$$

$$U_\phi \equiv \sin(2\phi)\frac{\lambda_6}{2i} + \cos(2\phi)\frac{\lambda_7}{2i}, \qquad U_\rho \equiv \cos(2\phi)\frac{\lambda_6}{2i} - \sin(2\phi)\frac{\lambda_7}{2i}, \qquad U_3 \equiv \frac{\sqrt{3}\lambda_8 - \lambda_3}{4i}, \tag{3.3c}$$

which have the property

$$\partial_\phi X = [-2U_3, X], \tag{3.4}$$

with X standing for any of the matrices defined in Eqs. (3.3a)–(3.3c).

The axial *Ansatz* functions $\alpha_i(r,\theta)$ have the following boundary conditions at the coordinate origin $(r = 0)$:

$$\alpha_i(0,\theta) = 0, \quad \text{for } i = 1,\ldots,8, \tag{3.5}$$

on the symmetry axis $(\bar{\theta} = 0, \pi)$:

$$\alpha_i(r,\bar{\theta}) = \tilde{\alpha}_i(r)\sin\theta|_{\theta=\bar{\theta}}, \quad \text{for } i = 1,2, \tag{3.6a}$$

$$\alpha_i(r,\bar{\theta}) = \tilde{\alpha}_i(r)\sin^2\theta|_{\theta=\bar{\theta}}, \quad \text{for } i = 3,4,5, \tag{3.6b}$$

$$\alpha_i(r,\bar{\theta}) = (-)^{i-5}\cos\theta\partial_\theta\alpha_{i-5}(r,\theta)|_{\theta=\bar{\theta}}, \quad \text{for } i = 6,7, \tag{3.6c}$$

$$\alpha_i(r,\bar{\theta}) = \frac{1}{2}\cos\theta\partial_\theta\alpha_{i-5}(r,\theta)|_{\theta=\bar{\theta}}, \quad \text{for } i = 8, \tag{3.6d}$$

and towards spatial infinity:

$$\lim_{r\to\infty}\begin{pmatrix}\alpha_1(r,\theta)\\ \alpha_2(r,\theta)\\ \alpha_3(r,\theta)\\ \alpha_4(r,\theta)\\ \alpha_5(r,\theta)\\ \alpha_6(r,\theta)\\ \alpha_7(r,\theta)\\ \alpha_8(r,\theta)\end{pmatrix}=\begin{pmatrix}-2\sin\theta(1+\sin^2\theta)\\ 2\sin\theta\cos^2\theta\\ -2\sin^2\theta\\ -\sin^2\theta(1+2\sin^2\theta)\\ \sqrt{3}\sin^2\theta\\ 2\\ 2\\ -2\sin\theta\end{pmatrix}. \tag{3.7}$$

The $\hat{S}$ Higgs fields are given by [3]

$$\begin{aligned}\hat{\Phi}(r,\theta,\phi)&=\eta[\beta_1(r,\theta)\lambda_3+\beta_2(r,\theta)\cos\theta 2iT_\rho\\ &\quad+\beta_3(r,\theta)2iV_\rho]\begin{pmatrix}1\\0\\0\end{pmatrix}\\ &=\eta\begin{pmatrix}\beta_1(r,\theta)\\ \beta_2(r,\theta)\cos\theta e^{i\phi}\\ \beta_3(r,\theta)e^{-i\phi}\end{pmatrix},\end{aligned} \tag{3.8}$$

with real functions $\beta_j(r,\theta)$ that are even under reflection of the z-coordinate,

$$\beta_j(r,\pi-\theta)=+\beta_j(r,\theta),\quad \text{for } j=1,2,3. \tag{3.9}$$

The axial *Ansatz* functions $\beta_j(r,\theta)$ have the following boundary conditions at the coordinate origin ($r=0$):

$$\beta_1(0,\theta)=\beta_2(0,\theta)=\beta_3(0,\theta)=0, \tag{3.10}$$

on the symmetry axis ($\bar{\theta}=0,\pi$):

$$\partial_\theta\beta_1(r,\theta)|_{\theta=\bar{\theta}}=0, \tag{3.11a}$$

$$\beta_j(r,\bar{\theta})=\tilde{\beta}_j(r)\sin\theta|_{\theta=\bar{\theta}},\quad \text{for } j=2,3, \tag{3.11b}$$

and towards spatial infinity:

$$\lim_{r\to\infty}\begin{pmatrix}\beta_1(r,\theta)\\ \beta_2(r,\theta)\\ \beta_3(r,\theta)\end{pmatrix}=\begin{pmatrix}\cos^2\theta\\ -\sin\theta\\ -\sin\theta\end{pmatrix}. \tag{3.12}$$

Note that boundary condition (3.10) is tighter than the one given in Ref. [3], which has only $\partial_\theta\beta_1(0,\theta)=0$. The boundary conditions (3.10) give a vanishing Higgs field at the origin, $\hat{\Phi}(0,\theta)=0$, which is needed for the existence of fermion zero modes if the theory (2.1) has additional Weyl fermions with Yukawa couplings to the Higgs (cf. Sec. V of the review article [10]). Recall that appropriate fermion zero modes give rise to the non-Abelian chiral gauge anomaly [1] as discussed in Refs. [2,3].

To summarize, the radial-gauge *Ansatz* for $\hat{S}$ in the basic YMH theory involves 11 axial functions, 8 functions $\alpha_i(r,\theta)$ for the Yang–Mills gauge fields and 3 functions $\beta_j(r,\theta)$ for the Higgs fields. The boundary conditions on α_i and β_j at spatial infinity make for vacuum-type fields with vanishing energy density and those at the coordinate origin and on the symmetry axis make for a finite energy density (see also Sec. IV B).

C. Energy functional

The energy functional of the YMH theory (2.1) is given by

$$E[A,\Phi]=\int_{\mathbb{R}^3}\mathrm{d}^3x\left[-\frac{1}{2}\mathrm{tr}(F_{mn})^2+|D_m\Phi|^2+\lambda(|\Phi|^2-\eta^2)^2\right], \tag{3.13}$$

where the spatial indices m, n run over 1, 2, 3. The $\hat{S}$ *Ansätze* (3.1) and (3.8) then give

$$E[\hat{A},\hat{\Phi}]=4\pi\int_0^\infty\mathrm{d}r\int_0^{\pi/2}\mathrm{d}\theta r^2\sin\theta\hat{e}(r,\theta), \tag{3.14}$$

where the energy density $\hat{e}(r,\theta)$ contains contributions from the Yang–Mills term, the kinetic Higgs term, and the Higgs potential term in the energy functional,

$$\hat{e}(r,\theta)=\hat{e}_{\mathrm{YM}}(r,\theta)+\hat{e}_{\mathrm{Hkin}}(r,\theta)+\hat{e}_{\mathrm{Hpot}}(r,\theta). \tag{3.15}$$

This energy density is given in Appendix A and turns out to be well-behaved due to the boundary conditions on the axial *Ansatz* functions $\alpha_i(r,\theta)$ and $\beta_j(r,\theta)$. The energy density has, moreover, a reflection symmetry,

$$\hat{e}(r,\theta)=\hat{e}(r,\pi-\theta), \tag{3.16}$$

which allows the range of θ in (3.14) to be restricted to $[0,\pi/2]$.

IV. FIELD EQUATIONS AND ANALYTICAL RESULTS

A. Reduced field equations

As shown in Ref. [3], and verified independently for the present article, the YMH field equations with $\hat{S}$ *Ansatz* fields inserted reduce to the variational equations obtained from the *Ansatz* energy functional (3.14). In short, the $\hat{S}$ *Ansatz* is self-consistent.

The variational equations (partial differential equations) from the *Ansatz* energy functional (3.14) are rather cumbersome and will not be given here (all the necessary information is contained in the energy density as given by Appendix A).

B. Analytic solution near the origin

The variational equations of Sec. IV A can be solved analytically near the origin ($r \sim 0$). Making the radial coordinate r dimensionless by multiplication with gv, the analytic solution of these partial differential equations near the origin ($r \sim 0$) gives the following *Ansatz* functions:

$$\begin{pmatrix} \alpha_1(r,\theta) \\ \alpha_2(r,\theta) \\ \alpha_3(r,\theta) \\ \alpha_4(r,\theta) \\ \alpha_5(r,\theta) \\ \alpha_6(r,\theta) \\ \cos^2\theta\alpha_7(r,\theta) \\ \alpha_8(r,\theta) \end{pmatrix} \sim \begin{pmatrix} c_1 r^2 \sin\theta \\ c_2 r^2 \sin\theta|\cos\theta| \\ c_3 r^3 \sin^2\theta \\ c_4 r^2 \sin^2\theta \\ c_5 r^2 \sin^2\theta \\ -c_1 r^2 \\ c_2 r^2|\cos\theta| \\ c_3 r^3 \sin\theta \end{pmatrix}, \tag{4.1a}$$

$$\begin{pmatrix} \beta_1(r,\theta) \\ \beta_2(r,\theta) \\ \beta_3(r,\theta) \end{pmatrix} \sim \begin{pmatrix} c_6 r|\cos\theta| \\ c_7 r^2 \sin\theta \\ c_8 r \sin\theta \end{pmatrix}, \tag{4.1b}$$

with constants $c_1, \ldots, c_8$. The functions (4.1), with nonzero constants c_k, make that the energy density at the origin is finite (positive) and regular (no θ dependence as $r \to 0$).

At this moment, recall the behavior of the *Ansatz* functions towards infinity ($r \to \infty$) as given by (3.7) and (3.12), but consider the combination $\cos^2\theta\alpha_7(r,\theta)$ instead of $\alpha_7(r,\theta)$. The remarkable observation is that the qualitative θ-behavior of these *Ansatz* functions [including the combination $\cos^2\theta\alpha_7(r,\theta)$] is similar towards the origin and towards infinity, provided $\{c_1, c_3, c_4, c_7, c_8\}$ are taken negative and $\{c_2, c_5, c_6\}$ positive. This observation underlies the useful redefinition of the *Ansatz* functions employed in Appendix B.

Equation (4.1b) gives the following behavior of the triplet Higgs field near the origin ($r \sim 0$):

$$\Phi_{\hat{S}}(x,y,z) \sim \eta \begin{pmatrix} c_6|z| \\ 0 \\ c_8(x-iy) \end{pmatrix}, \tag{4.2}$$

with dimensionless Cartesian coordinates and the second component being $\mathrm{O}(r^2)$ for $r^2 \equiv x^2 + y^2 + z^2$. The Higgs field (4.2) shows a cusp-like behavior for the first component. Still, the energy density involving the Higgs field is well-behaved near the origin. For comparison, the $SU(2)$ sphaleron S [4] has the following behavior of the doublet Higgs field near the origin (again with dimensionless Cartesian coordinates):

$$\Phi_S(x,y,z) \sim \frac{v}{\sqrt{2}} c_h \begin{pmatrix} x+iy \\ z \end{pmatrix}, \tag{4.3}$$

which is perfectly smooth.

We can provide the following heuristic explanation of the different behavior of the S and $\hat{S}$ Higgs fields at the origin. If the Higgs behavior near the origin is given by $\Phi \propto r$, then S gets a component $c_h z$ because the corresponding $\cos\theta$ behavior at infinity is odd under $\theta \to \pi - \theta$, whereas $\hat{S}$ gets a component $c_6|z|$ because the corresponding $\cos^2\theta$ behavior at infinity is even.

V. NUMERICAL RESULTS

A. Minimization setup

In order to apply numerical minimization techniques, we approximate the energy functional (3.14) by an energy function of expansion coefficients, where the relevant energy density (3.15) has been detailed in Appendix A. For this, we expand the two-dimensional profile functions $\alpha_i(r,\theta)$ and $\beta_j(r,\theta)$ in nested orthogonal functions, as done in previous work [11–13] on the $\hat{S}$ numerics.

For the radial expansion, we switch to a compact radial coordinate x defined by

$$x \equiv \frac{gvr}{\chi + gvr} \in [0,1], \tag{5.1a}$$

$$\chi \in \mathbb{R}^+, \tag{5.1b}$$

with $v \equiv \sqrt{2}\eta$ as mentioned in Sec. II A. The other coordinate, the polar angle θ, is compact by definition and can be restricted to the following domain by use of the reflection symmetry:

$$\theta \in [0, \pi/2]. \tag{5.2}$$

The details of the expansion coefficients for the *Ansatz* functions are relegated to Appendix B.

The double expansion in x and θ of the *Ansatz* functions gives asymptotically (M, $N \to \infty$) the following total number of coefficients from (B11):

$$N_{\text{coeff}}^{(\text{basic YMHth})} \sim 22NM. \tag{5.3}$$

The asymptotic behavior (5.3) can be understood as follows: 11 *Ansatz* functions (8 for the gauge fields and 3 for the Higgs fields), a factor $(2N+1) \sim 2N$ from the θ-expansion (B4), and a factor $(M+1) \sim M$ from the x-expansion (B9).

B. Numerical solution

The *Ansatz*-function expansions presented in Appendix B produce the $\hat{S}$ energy as a function of the expansion coefficients. The task, now, is to find the optimal coefficients

for an energy minimum (recall that finding the perfect coefficients corresponds to solving the reduced field equations).

As a first step, we employ the simulated annealing (SA) method [14], a randomized global minimizer to give, within a reasonable runtime, the best possible set of initial values for the second step. That second step is a quadratically-convergent local minimizer based on the Sequential Least-Squares Quadratic Programming (SLSQP) method [15].

For our numerical calculations, a C++ program of the first SA step has been written from the ground up, as an alternative to using one from the many available libraries. The program of the second step relies upon the SLSQP implementation of the Python library SciPy [16].

As the analytic integrations of the energy functional are typically not feasible due to the size, the integrations over x and θ must be carried out numerically. The numerical integrations over x and θ are done with the composite Simpson's rule over a mesh given by the nodes of Chebyshev polynomials of sufficiently large degree. This choice of grid spacing is known to minimize the effect of Runge's phenomenon, which occurs if the grid size does not exceed the expansion order by much. [As a check of these numerical integrations, we have also performed analytic integrations for relatively low expansion orders, the largest being $(M, N) = (3, 1)$ with some 2.3×10^6 summands in the resulting energy function.]

For $\lambda/g^2 = 0$ and various expansion cutoffs M and N, we find the energies listed in Table I. From this table, we obtain the following value of the $\hat{S}$ energy:

$$E_{\hat{S}}^{(\text{basic } SU(3) \text{ YMHth}, \lambda/g^2=0)} = (1.35 \pm 0.03) \times (4\pi v/g), \quad (5.4)$$

with a rough error estimate obtained from combining the relative differences of energy values in the last three rows of Table I and the numerical relative error mentioned in the table caption. For expansion cutoffs $M = 18$ and $N = 3$, the energy densities are shown in Figs. 1 and 2. The corresponding *Ansatz* functions are not shown, as certain gauge boson modes of the basic $SU(3)$ YMH theory are massless and the convergence is slow. [As the *Ansatz* functions are not perfectly converged, the contours of Fig. 1 also need to be smoothed somewhat, especially near the symmetry axis $(x = y = 0)$ and the equatorial plane

TABLE I. Numerical estimates of the energy value of the sphaleron $\hat{S}$ in the basic $SU(3)$ Yang–Mills–Higgs theory (2.1) with $\lambda/g^2 = 0$ and definition $v \equiv \sqrt{2}\eta$. The different energy values are obtained from numerical minimization with various expansion cutoffs M and N, where the parameter $\chi = 5$ is used for the radial compactification (5.1). A conservative estimate of the numerical error on the energies quoted is $10^{-2} 4\pi v/g$.

M	N	$E_{\hat{S}}/[4\pi v/g]$
3	1	1.610
6	1	1.468
6	2	1.433
11	2	1.371
11	3	1.360
18	3	1.345

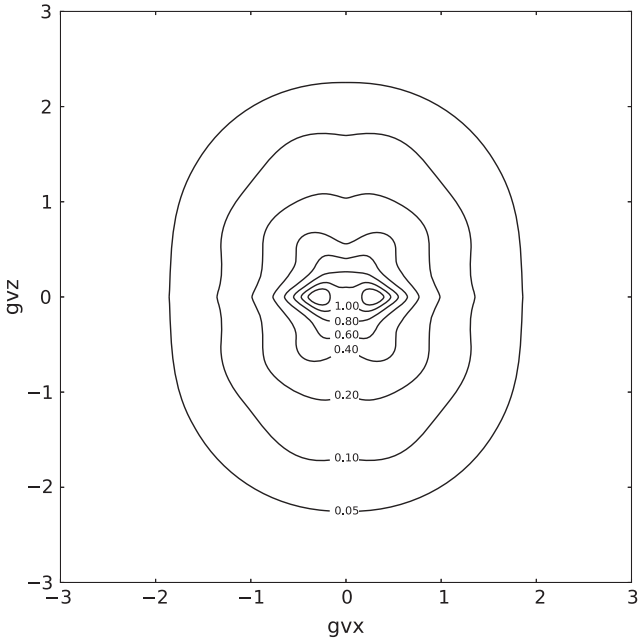

FIG. 1. Energy density (3.15) of the numerical $\hat{S}$ solution in the basic $SU(3)$ Yang–Mills–Higgs theory (2.1) for $\lambda/g^2 = 0$ and $v \equiv \sqrt{2}\eta$. The numerical solution is obtained from minimization with expansion cutoffs $N = 3$ and $M = 18$, for a radial-compactification parameter $\chi = 5$. Cartesian coordinates (x, y, z) are used and the plane $y = 0$ is shown. The two small contours around $(gvx, gvz) = (\pm 0.3, 0)$ have the energy-density value 1.20, in units of $(4\pi v/g)(gv)^3$.

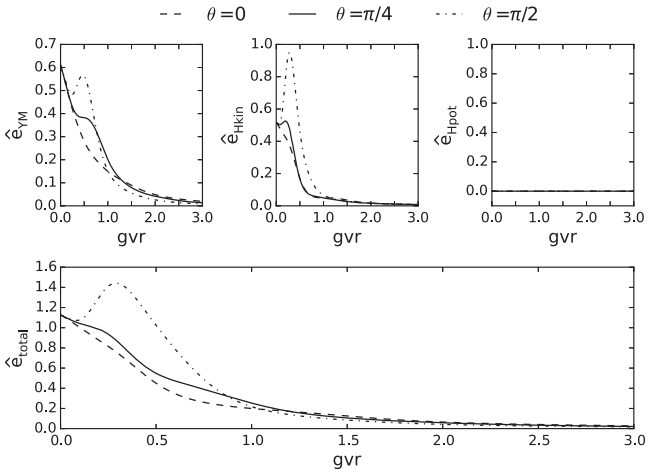

FIG. 2. Same as Fig. 1, but now for three slices at fixed polar angle θ and showing the various contributions to the total energy density, with $\hat{e}_{\text{Hpot}} = 0$ for $\lambda/g^2 = 0$.

$(z = 0)$.] For the extended theory, all gauge boson modes are massive and the convergence is better (see Sec. VI C).

The $\hat{S}$ energy distribution of Fig. 1 shows a nontrivial core ($gvr \lesssim 0.75$), but the suggested ring structure (with center at $gvr \sim 0.3$ in the $\theta = \pi/2$ plane) needs to be confirmed by further calculations. Somewhat further out ($1 \lesssim gvr \lesssim 2$), and with respect to the axial-symmetry axis (the z-axis in our coordinate system), the energy distribution is slightly prolate (equatorial radius smaller than polar radius). The main contribution to the total energy comes from $gvr \sim 4$.

C. Discussion

The result for the energy $E_{\hat{S}}$ obtained in Sec. V B may be compared to the energy E_S of the embedded $SU(2) \times U(1)$ sphaleron S, which has the following value (cf. Table 1 of Ref. [5] and Fig. 1 of Ref. [6]):

$$E_S^{(\theta_w=\pi/6,\lambda/g^2=0)} \approx 1.505 \times (4\pi v/g), \tag{5.5}$$

where we used $v \equiv \sqrt{2}\eta$ as mentioned in Sec. II A. With the numerical result (5.4) for the $\hat{S}$ energy at $\lambda/g^2 = 0$, we then have the following ratio:

$$E_{\hat{S}}^{(\lambda/g^2=0)}/E_S^{(\theta_w=\pi/6,\lambda/g^2=0)} \approx 0.90, \tag{5.6}$$

which is definitely below unity. (Hints of an $E_{\hat{S}}/E_S$ ratio below unity were, first, reported in Ref. [11] and, later, in Refs. [12,13]. The behavior of the $\hat{S}$ fields near the origin was, however, not correct in these earlier numerical calculations.)

The result (5.6) is remarkable in that the $\hat{S}$ solution excites all eight gauge fields and the S solution only four. The low energy value of $\hat{S}$ is, most likely, due to the fact that the *Ansatz* (3.1) has azimuthal and polar gauge fields which are evenly distributed over the Lie algebra.

VI. $\hat{S}$ IN THE EXTENDED $SU(3)$ YMH THEORY

The construction of $\hat{S}$ in the extended $SU(3)$ Yang–Mills–Higgs theory (2.8) follows that of $\hat{S}$ in the basic $SU(3)$ Yang–Mills–Higgs theory (2.1) as given in Ref. [3] and we can be relatively brief as regards the motivation of the *Ansatz*. As explained in Sec. III A, the crucial element for the $\hat{S}$ *Ansatz* is a noncontractible sphere of configurations, which, for the extended $SU(3)$ Yang–Mills–Higgs theory, is presented in Appendix C.

A. $\hat{S}$ Ansatz

The proper *Ansatz* for $\hat{S}$ in the extended $SU(3)$ YMH theory (2.8) corresponds to a generalization of the fields (C6) at the "top" ($\psi = \pi$) of the noncontractible sphere of configurations constructed in Appendix C.

For the radial gauge, the *Ansatz* gauge fields $\hat{A}$ are again given by (3.1) and the *Ansatz* Higgs fields $\hat{\Phi}_\alpha$ correspond to appropriate generalizations of the fields in Eqs. (C6c)–(C6e):

$$\hat{\Phi}_1(r,\theta,\phi) = \eta \begin{pmatrix} \beta_1(r,\theta) \\ \cos\theta\beta_2(r,\theta)e^{i\phi} \\ \beta_3(r,\theta)e^{-i\phi} \end{pmatrix}, \tag{6.1a}$$

$$\hat{\Phi}_2(r,\theta,\phi) = \eta \begin{pmatrix} \beta_4(r,\theta)e^{-i\phi} \\ \cos\theta\beta_5(r,\theta) \\ \beta_6(r,\theta) \end{pmatrix}, \tag{6.1b}$$

$$\hat{\Phi}_3(r,\theta,\phi) = \eta \begin{pmatrix} \cos\theta\beta_7(r,\theta)e^{i\phi} \\ \beta_8(r,\theta)e^{2i\phi} \\ \cos\theta\beta_9(r,\theta) \end{pmatrix}, \tag{6.1c}$$

with real functions $\beta_k(r,\theta)$ that are even under reflection of the z-coordinate,

$$\beta_k(r,\pi-\theta) = +\beta_k(r,\theta), \quad \text{for } k = 1,\ldots,9. \tag{6.2}$$

The *Ansatz* (6.1a) for the first triplet is the same as (3.8) for the basic $SU(3)$ YMH theory. In addition, there are the following boundary conditions at the origin and toward infinity

$$\beta_k(0,\theta) = 0, \quad \text{for } k = 1,\ldots,9, \tag{6.3a}$$

$$\lim_{r\to\infty} \begin{pmatrix} \beta_1(r,\theta) \\ \beta_2(r,\theta) \\ \beta_3(r,\theta) \\ \beta_4(r,\theta) \\ \beta_5(r,\theta) \\ \beta_6(r,\theta) \\ \beta_7(r,\theta) \\ \beta_8(r,\theta) \\ \beta_9(r,\theta) \end{pmatrix} = \begin{pmatrix} \cos^2\theta \\ -\sin\theta \\ -\sin\theta \\ -\sin\theta \\ -1 \\ 0 \\ -\sin\theta \\ \sin^2\theta \\ -1 \end{pmatrix}, \tag{6.3b}$$

and the following boundary conditions on the symmetry axis ($\bar{\theta} = 0, \pi$):

$$\partial_\theta\beta_1(r,\theta)|_{\theta=\bar{\theta}} = 0, \quad \text{for } k = 1,5,6,9, \tag{6.4a}$$

$$\beta_k(r,\theta)|_{\theta=\bar{\theta}} = \tilde{\beta}_k(r)\sin\theta|_{\theta=\bar{\theta}}, \quad \text{for } k = 2,3,4,7, \tag{6.4b}$$

$$\beta_8(r,\theta)|_{\theta=\bar{\theta}} = \tilde{\beta}_8(r)\sin^2\theta|_{\theta=\bar{\theta}}. \tag{6.4c}$$

To summarize, the radial-gauge *Ansatz* for $\hat{S}$ in the extended YMH theory involves 17 axial functions, 8

functions $\alpha_i(r,\theta)$ for the Yang–Mills gauge fields and 9 functions $\beta_k(r,\theta)$ for the Higgs fields. Again, the boundary conditions on α_i and β_k at spatial infinity make for vacuum-type fields with vanishing energy density and those at the coordinate origin and on the symmetry axis make for a finite energy density.

B. Analytic solution near the origin

The energy density from the $\hat{S}$ *Ansätze* (3.1) and (6.1) in the extended YMH theory is given in Appendix D. The corresponding variational equations have the following solution near the origin ($r \sim 0$):

$$\begin{pmatrix} \beta_4(r,\theta) \\ \beta_5(r,\theta) \\ \beta_6(r,\theta) \\ \beta_7(r,\theta) \\ \beta_8(r,\theta) \\ \beta_9(r,\theta) \end{pmatrix} \sim \begin{pmatrix} -a_9 r \sin\theta \\ -a_{10} r \\ a_{11} r |\cos\theta| \\ -a_{12} r^2 \sin\theta \\ a_{13} r^2 \sin^2\theta \\ -a_{14} r \end{pmatrix}, \tag{6.5}$$

where some suggestive minus signs have been inserted, so that the qualitative θ-behavior at the origin matches the behavior (6.3b) at infinity. The solutions for the other eleven *Ansatz* functions near the origin have already been given in (4.1).

C. Numerical solution

The numerical minimization of the $\hat{S}$ energy in the extended YMH theory parallels the calculation in the basic YMH theory and is summarized in Appendix E. The double expansion in x and θ of the *Ansatz* functions gives asymptotically ($M, N \to \infty$) the following total number of coefficients from (E10):

$$N_{\text{coeff}}^{(\text{ext YMHth})} \sim 34NM. \tag{6.6}$$

The asymptotic behavior (6.6) can be understood as follows: 17 *Ansatz* functions (8 for the gauge fields and 9 for the Higgs fields), a factor $(2N+1) \sim 2N$ from the θ-expansion, and a factor $(M+1) \sim M$ from the x-expansion.

For $\lambda/g^2 = 1$ and various expansion cutoffs M and N, we obtain the energies listed in Table II. From this table, we obtain the following value of the $\hat{S}$ energy:

$$E_{\hat{S}}^{(\text{ext } SU(3) \text{ YMHth}, \lambda/g^2=1)} = (8.50 \pm 0.03) \times (4\pi\eta/g), \tag{6.7}$$

with a rough error estimate obtained from combining the relative difference of energy values in the last three rows of Table II and the numerical relative error mentioned in the table caption. The various contributions to the total energy have, for the $(M,N) = (11,3)$ numerical solution, the approximate ratios $E_{\text{YM}} : E_{\text{Hkin}} : E_{\text{Hpot}} \approx 0.532 : 0.384 : 0.084$ and the corresponding energy densities are shown in Figs. 3 and 4. The main contribution to the total energy comes from $gvr \sim 1.5$ (see Table III for the build-up of the total energy).

TABLE II. Numerical estimates of the energy value of the sphaleron $\hat{S}$ in the extended $SU(3)$ Yang–Mills–Higgs theory (2.8) with $\lambda/g^2 = 1$ and $v \equiv \sqrt{2}\eta$. The different energy values are obtained from numerical minimization with various expansion cutoffs M and N, where the parameter $\chi = 3/2$ is used for the radial compactification (5.1). A conservative estimate of the numerical error on the energies quoted is $10^{-2} 4\pi\eta/g$.

M	N	$E_{\hat{S}}/[4\pi\eta/g]$
3	1	8.627
6	1	8.527
6	2	8.526
11	2	8.506
11	3	8.503

Figures 3 and 4 make clear that, with respect to the axial-symmetry axis (the z-axis in our coordinate system), the $\hat{S}$ energy distribution for $gvr \gtrsim 0.6$ is slightly oblate (equatorial radius larger than polar radius), whereas the energy distribution for $gvr \lesssim 0.4$ appears to be slightly prolate.

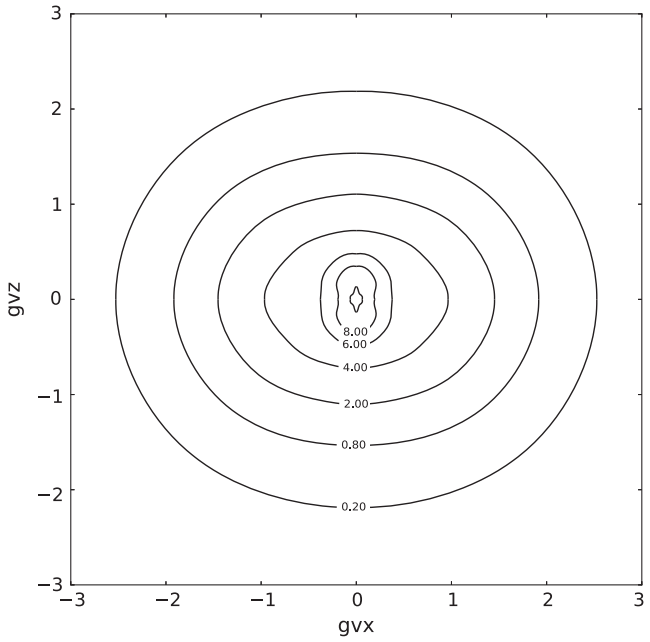

FIG. 3. Energy density (D1) of the numerical $\hat{S}$ solution in the extended $SU(3)$ Yang–Mills–Higgs theory (2.8) for $\lambda/g^2 = 1$ and $v \equiv \sqrt{2}\eta$. The numerical solution is obtained from minimization with expansion cutoffs $N = 3$ and $M = 11$, for a radial-compactification parameter $\chi = 3/2$. Cartesian coordinates (x,y,z) are used and the plane $y = 0$ is shown. The small contour around $(gvx, gvz) = (0,0)$ has the energy-density value 8.00, in units of $(4\pi v/g)(gv)^3$.

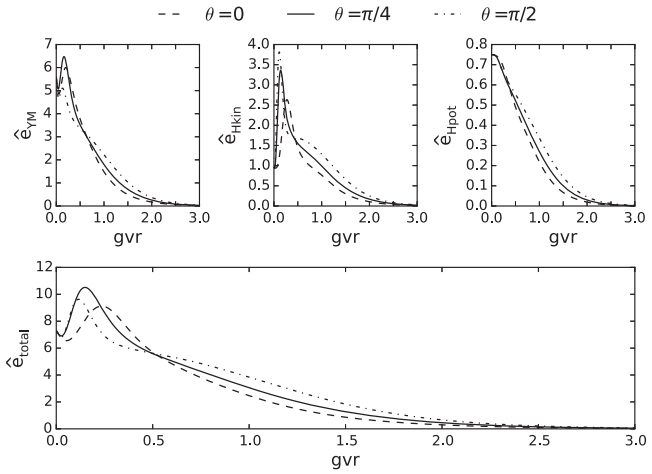

FIG. 4. Same as Fig. 3, but now for three slices at fixed polar angle θ and showing the various contributions to the total energy density.

In order to show the profile functions $\alpha_i(x,\theta)$ and $\beta_k(x,\theta)$ of the numerical solution, we introduce the following rescalings with angular functions:

$$\begin{pmatrix} \hat{\alpha}_1(x,\theta) \\ \hat{\alpha}_2(x,\theta) \\ \hat{\alpha}_3(x,\theta) \\ \hat{\alpha}_4(x,\theta) \\ \hat{\alpha}_5(x,\theta) \\ \hat{\alpha}_6(x,\theta) \\ \hat{\alpha}_7(x,\theta) \\ \hat{\alpha}_8(x,\theta) \end{pmatrix} = \begin{pmatrix} \alpha_1(x,\theta)/[-2\sin\theta(1+\sin^2\theta)] \\ \alpha_2(x,\theta)/[2\sin\theta] \\ \alpha_3(x,\theta)/[-2\sin^2\theta] \\ \alpha_4(x,\theta)/[-\sin^2\theta(1+2\sin^2\theta)] \\ \alpha_5(x,\theta)/[\sqrt{3}\sin^2\theta] \\ \alpha_6(x,\theta)/2 \\ \alpha_7(x,\theta)/2 \\ \alpha_8(x,\theta)/[-2\sin\theta] \end{pmatrix}, \tag{6.8a}$$

$$\begin{pmatrix} \hat{\beta}_1(x,\theta) \\ \hat{\beta}_2(x,\theta) \\ \hat{\beta}_3(x,\theta) \\ \hat{\beta}_4(x,\theta) \\ \hat{\beta}_5(x,\theta) \\ \hat{\beta}_6(x,\theta) \\ \hat{\beta}_7(x,\theta) \\ \hat{\beta}_8(x,\theta) \\ \hat{\beta}_9(x,\theta) \end{pmatrix} = \begin{pmatrix} \beta_1(x,\theta) \\ \beta_2(x,\theta)/[-\sin\theta] \\ \beta_3(x,\theta)/[-\sin\theta] \\ \beta_4(x,\theta)/[-\sin\theta] \\ -\beta_5(x,\theta) \\ \beta_6(x,\theta) \\ \beta_7(x,\theta)/[-\sin\theta] \\ \beta_8(x,\theta)/[\sin^2\theta] \\ -\beta_9(x,\theta) \end{pmatrix}, \tag{6.8b}$$

where the divisions by $\sin\theta$ or $\sin^2\theta$ are allowed by the boundary conditions on the symmetry axis, as given by Eqs. (3.6) and (6.4). For these redefined *Ansatz* functions, the behavior at spatial infinity is simplified, with values in the range [0, 1],

TABLE III. Energy contribution up to radius R of the numerical $\hat{S}$ solution in the extended $SU(3)$ Yang–Mills–Higgs theory (2.8) for $\lambda/g^2 = 1$ and $v \equiv \sqrt{2}\eta$. The numerical solution has been obtained from minimization with expansion cutoffs $N = 3$ and $M = 11$ using $\chi = 3/2$. The values of the partial energy $\hat{E}_R \equiv 4\pi \int_0^R dr \int_0^{\pi/2} d\theta r^2 \sin\theta \hat{e}(r,\theta)$ are given relative to the total energy $\hat{E}_\infty = E_{\hat{S}}$ from Table II.

gvR	$\hat{E}_R/\hat{E}_\infty$
0.3	0.0125
0.6	0.0719
0.9	0.1923
1.2	0.3574
1.5	0.5252
1.8	0.6785
2.1	0.7840
2.4	0.8649
2.7	0.9120
3.0	0.9449
4.0	0.9870
5.0	0.9958
6.0	0.9979

$$\lim_{x\to 1} \begin{pmatrix} \hat{\alpha}_1(x,\theta) \\ \hat{\alpha}_2(x,\theta) \\ \hat{\alpha}_3(x,\theta) \\ \hat{\alpha}_4(x,\theta) \\ \hat{\alpha}_5(x,\theta) \\ \hat{\alpha}_6(x,\theta) \\ \cos^2\theta\hat{\alpha}_7(x,\theta) \\ \hat{\alpha}_8(x,\theta) \end{pmatrix} = \begin{pmatrix} 1 \\ \cos^2\theta \\ 1 \\ 1 \\ 1 \\ 1 \\ \cos^2\theta \\ 1 \end{pmatrix}, \tag{6.9a}$$

$$\lim_{x\to 1} \begin{pmatrix} \hat{\beta}_1(x,\theta) \\ \hat{\beta}_2(x,\theta) \\ \hat{\beta}_3(x,\theta) \\ \hat{\beta}_4(x,\theta) \\ \hat{\beta}_5(x,\theta) \\ \hat{\beta}_6(x,\theta) \\ \hat{\beta}_7(x,\theta) \\ \hat{\beta}_8(x,\theta) \\ \hat{\beta}_9(x,\theta) \end{pmatrix} = \begin{pmatrix} \cos^2\theta \\ 1 \\ 1 \\ 1 \\ 1 \\ 0 \\ 1 \\ 1 \\ 1 \end{pmatrix}. \tag{6.9b}$$

The boundary conditions at the origin match (3.5) and (6.3a) of the original *Ansatz* functions,

$$\hat{\alpha}_i(0,\theta) = 0, \quad \text{for } i = 1,\ldots,8, \tag{6.10a}$$

$$\hat{\beta}_k(0,\theta) = 0, \quad \text{for } k = 1,\ldots,9. \tag{6.10b}$$

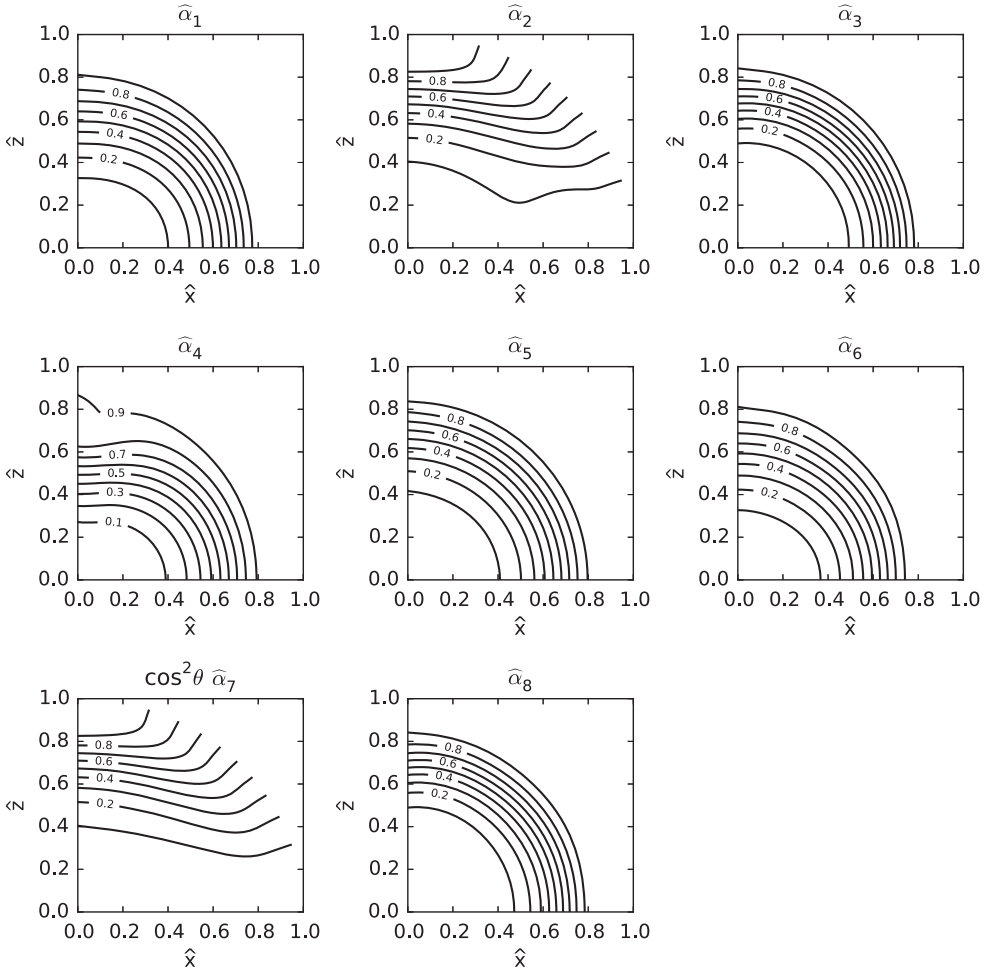

FIG. 5. Equidistant contour plots of the rescaled profile functions $\hat{\alpha}_i(x,\theta)$ of the $(M,N)=(11,3)$ configuration obtained from numerical minimization of the $\hat{S}$ energy functional in the extended Yang-Mills-Higgs theory (2.8) for $\lambda/g^2=1$. The rescaled profile functions $\hat{\alpha}_i(x,\theta)$ are defined by (6.8a). Compactified Cartesian coordinates $(\hat{x},\hat{y},\hat{z})$ are used and the plane $\hat{y}=0$ is displayed. Specifically, the two coordinates shown are given by $\hat{x}=gvr\sin\theta/(gvr+\chi)$ and $\hat{z}=gvr\cos\theta/(gvr+\chi)$. The numerical minimization procedure and the contour plots both use $\chi=3/2$.

Figures 5 and 6 present the rescaled profile functions of the numerical solution. As mentioned in the caption of Fig. 6, the numerical solution for $\hat{\beta}_6(x,\theta)=\beta_6(x,\theta)$ is close to zero. It can, indeed, be shown that $\beta_6(x,\theta)=0$ solves the β_6 variational equation from (D2a) and (D3). With all Yang-Mills modes massive, the energy densities and profile functions appear to have converged reasonably well, but the detailed behavior of Figs. 3–6 may still change somewhat with further minimization runs.

D. Discussion

The $\hat{S}$ gauge fields in the extended $SU(3)$ YMH theory have a very special structure (as mentioned in the last paragraph of Sec. V C) and we conjecture that these gauge fields may somehow play a role in the nonperturbative dynamics of QCD. It is true that the Higgs fields are important for obtaining an equilibrium solution (E_{YM} scales as $1/\bar{R}$ and E_{Hkin} scales as $\bar{R}$, with $\bar{R}$ the typical scale of the configuration). In QCD, there are no such fundamental Higgs fields and it is not clear how the $\hat{S}$ gauge fields would be prevented from expanding ($\bar{R}\to\infty$). Still, it is not excluded that QCD quantum effects produce attractive forces on this special lump of gauge fields. In any case, it appears that the Yang-Mills configuration space near the $\hat{S}$ gauge field configuration is relatively flat and this static three-dimensional configuration may play a role in a Hamiltonian analysis. (The corresponding instanton-type configuration $\hat{I}$ [which has NCS gauge fields (C3a) and (C3b) with $\psi=\psi(t)$ and, for example, $\mu=\alpha=\pi/2$] may play a role in the Euclidean path integral.)

The result for the energy $E_{\hat{S}}$ obtained in Sec. VI C can be compared to the following nonperturbative "soliton" energy scale:

$$E_{\text{gl,soliton}}\equiv m_{\text{gl}}/\alpha_{\text{gl}}, \tag{6.11a}$$

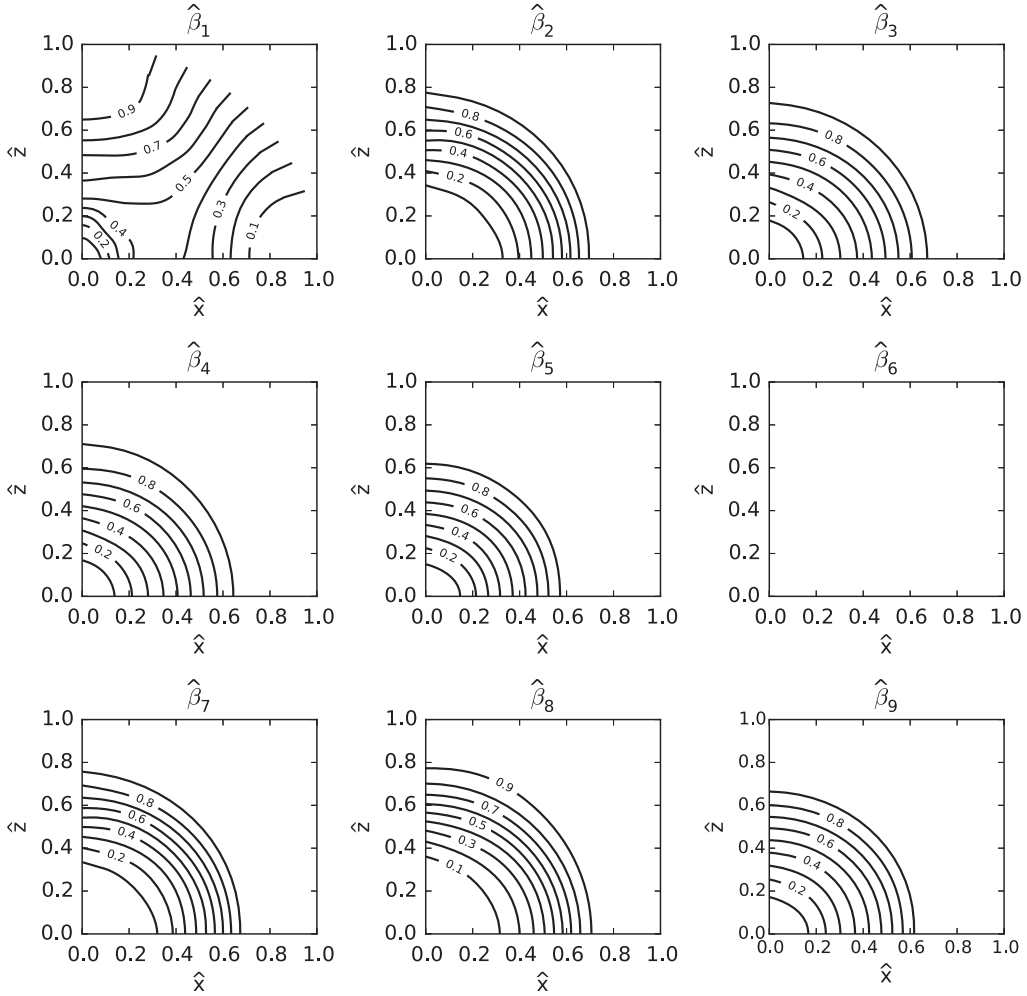

FIG. 6. Same as Fig. 5, but now with equidistant contour plots of the rescaled profile functions $\hat{\beta}_k(x,\theta)$ from (6.8b). The numerical result for $\hat{\beta}_6$ is close to zero, $|\hat{\beta}_6| \lesssim 3\times 10^{-4}$.

defined in terms of the "gluon mass" and the "gluon fine-structure constant,"

$$m_{\rm gl} \equiv g\eta, \tag{6.11b}$$

$$\alpha_{\rm gl} \equiv g^2/(4\pi), \tag{6.11c}$$

where the last two right-hand-sides involve quantities of our classical extended $SU(3)$ YMH theory (2.8). With the numerical result (6.7) for the $\hat{S}$ energy, we then have the following ratio:

$$E_{\hat{S}}/E_{\rm gl,soliton} \approx 8.5. \tag{6.12}$$

Another characteristic of $\hat{S}$ is its size. Table III shows that the radius for which the energy has reached 90% of its asymptotic value is approximately $2.60/(gv) \approx 1.84/(g\eta)$ and the corresponding diameter is then

$$d_{\hat{S}} \approx \frac{3.7}{m_{\rm gl}}, \tag{6.13}$$

where $m_{\rm gl}$ has been defined by (6.11b).

With the cautionary remarks of the first paragraph of this subsection in mind, we now turn to QCD and consider the $\hat{S}$ gauge fields obtained in Sec. VI C. From QCD, we take over $m_{\rm gl} \sim ({\rm fm})^{-1} \sim 200$ MeV and $\alpha_{\rm gl} \sim \alpha_s(200\,{\rm MeV}) \sim 1$ (cf. Fig. 9.3 of Ref. [8]), so that $E_{\rm gl,soliton} \sim 200$ MeV. Then, ratio (6.12) gives $E_{\hat{S}} \sim 8.5 \times 200$ MeV ~ 1.7 GeV in a QCD context. Similarly, the $\hat{S}$ diameter (6.13) would correspond to 3.7 fm in a QCD context and Fig. 3 would give the energy-density contours (scaled by a factor of $1/2$ perhaps) for Cartesian coordinates x and z in units of 0.71 fm. We conjecture that the $\hat{S}$ gauge fields (with an energy of order 0.8 GeV perhaps) may contribute substantially to the field content of QCD glueballs (cf. p. 798 of Ref. [8]).

Let us place our suggestion about QCD glueballs in context. It is, by now, well-known that, in an effective

meson theory (motivated by QCD with an infinitely large number N_c of colors [17]), baryons may be considered as solitons [18–20]. But there appears to be no place for glueballs in this effective meson theory. For this reason, we suggest to use the extended $SU(3)$ YMH theory (2.8) as a complementary effective theory, without mesons and baryons, but possibly with glueballs as solitons/sphalerons. Admittedly, the extended $SU(3)$ YMH theory would not have linear (flux-tube) confinement of gluons, but the gauge bosons would be massive and not reach far out. A more serious problem is the apparent lack of a small parameter in QCD, which would support the use of semiclassical methods in the effective YMH theory.

VII. CONCLUSION

In this article, we have obtained the numerical solutions of the sphaleron $\hat{S}$ in two $SU(3)$ Yang–Mills–Higgs theories, one with a single Higgs triplet and another with three Higgs triplets. There were two crucial steps in getting these numerical results. The first step was that we managed to obtain the respective analytic solutions of the *Ansatz* functions near the coordinate origin. The second step was to use a mixed analytical-numerical procedure, namely, to expand the *Ansatz* functions in orthogonal polynomials, to perform the energy integrals analytically for low expansion orders or numerically for larger expansion orders, and, finally, to use an efficient numerical minimization procedure over the expansion coefficients in the remaining expression for the energy.

There are, at least, three outstanding issues. The first issue is to numerically obtain the corresponding fermion zero modes, based on the *Ansätze* of Ref. [3]. The second issue is to perform the stability analysis of the $\hat{S}$ solutions found in the two $SU(3)$ Yang–Mills–Higgs theories considered. The third issue is, depending on the outcome of this stability analysis ($\hat{S}$ being unstable or perhaps metastable), to determine the proper role of the $\hat{S}$ gauge fields in the nonperturbative dynamics of quarkless quantum chromodynamics.

ACKNOWLEDGMENTS

FRK thanks J. Greensite for useful discussions on QCD.

APPENDIX A: $\hat{S}$ ENERGY DENSITY IN THE BASIC $SU(3)$ YMH THEORY

In this appendix, we present the $\hat{S}$ energy density (3.15) of the radial-gauge *Ansatz* fields (3.1) and (3.8) in the basic $SU(3)$ Yang–Mills–Higgs theory (2.1). The following expressions are, in fact, equivalent to the energy densities from Ref. [3] for $\alpha_9 = \alpha_{10} = \alpha_{11} = 0$:

$$\begin{aligned}
\hat{e}_{\text{YM}} = {}& \frac{1}{2g^2r^2\sin^2\theta}\{\cos^2\theta(\partial_r\alpha_1)^2 + (\partial_r\alpha_2)^2 + \cos^2\theta(\partial_r\alpha_3)^2 + (\partial_r\alpha_4)^2 + (\partial_r\alpha_5)^2\} \\
& + \frac{1}{2g^2r^2}\{(\partial_r\alpha_6)^2 + \cos^2\theta(\partial_r\alpha_7)^2 + (\partial_r\alpha_8)^2\} \\
& + \frac{1}{2g^2r^4\sin^2\theta}\left\{\left[\partial_\theta(\cos\theta\alpha_1) + \alpha_6 - \frac{1}{2}\alpha_2\alpha_8 + \alpha_4\alpha_6 - \frac{1}{2}\cos^2\theta\alpha_3\alpha_7\right]^2\right. \\
& + \left[\partial_\theta\alpha_2 - \cos\theta\alpha_7 - \frac{1}{2}\cos\theta(\alpha_3\alpha_6 - \alpha_1\alpha_8 - \sqrt{3}\alpha_5\alpha_7 - \alpha_4\alpha_7)\right]^2 \\
& + \left[\partial_\theta(\cos\theta\alpha_3) - 2\alpha_8 - \frac{1}{2}\alpha_4\alpha_8 + \frac{1}{2}\alpha_2\alpha_6 + \frac{1}{2}\sqrt{3}\alpha_5\alpha_8 + \frac{1}{2}\cos^2\theta\alpha_1\alpha_7\right]^2 \\
& \left. + \left[\partial_\theta\alpha_4 - \cos\theta\left(\alpha_1\alpha_6 + \frac{1}{2}\alpha_2\alpha_7 - \frac{1}{2}\alpha_3\alpha_8\right)\right]^2 + \left[\partial_\theta\alpha_5 - \frac{\sqrt{3}}{2}\cos\theta(\alpha_3\alpha_8 + \alpha_2\alpha_7)\right]^2\right\},
\end{aligned} \tag{A1}$$

$$\begin{aligned}
\hat{e}_{\text{Hkin}} = {}& \eta^2\{(\partial_r\beta_1)^2 + \cos^2\theta(\partial_r\beta_2)^2 + (\partial_r\beta_3)^2\} \\
& + \frac{\eta^2}{r^2}\left\{\left[\partial_\theta\beta_1 - \frac{1}{2}\cos\theta(\alpha_7\beta_3 + \alpha_6\beta_2)\right]^2 + \left[\partial_\theta(\cos\theta\beta_2) + \frac{1}{2}(\alpha_6\beta_1 - \alpha_8\beta_3)\right]^2 + \left[\partial_\theta\beta_3 + \frac{1}{2}\cos\theta(\alpha_8\beta_2 + \alpha_7\beta_1)\right]^2\right\} \\
& + \frac{\eta^2}{4r^2\sin^2\theta}\{[\alpha_4\beta_1 + \alpha_5\beta_1/\sqrt{3} + \cos^2\theta\alpha_1\beta_2 + \alpha_2\beta_3]^2 + \cos^2\theta[2\beta_2 - \alpha_1\beta_1 + \alpha_4\beta_2 - \alpha_5\beta_2/\sqrt{3} - \alpha_3\beta_3]^2 \\
& + [2\beta_3 + \alpha_2\beta_1 - 2\alpha_5\beta_3/\sqrt{3} + \cos^2\theta\alpha_3\beta_2]^2\},
\end{aligned} \tag{A2}$$

$$\hat{e}_{\text{Hpot}} = \lambda\eta^4(\beta_1^2 + \cos^2\theta\beta_2^2 + \beta_3^2 - 1)^2. \tag{A3}$$

APPENDIX B: EXPANSION COEFFICIENTS FOR THE ANSATZ FUNCTIONS IN THE BASIC $SU(3)$ YMH THEORY

In this appendix, we give the details of the double expansion of the $\hat{S}$ *Ansatz* functions. In view of the behavior (4.1) at the origin and the boundary conditions (3.7) and (3.12) towards spatial infinity, we redefine the two-dimensional profile functions of the generalized *Ansatz* as follows:

$$\begin{pmatrix} \bar{\alpha}_1(x,\theta) \\ \bar{\alpha}_2(x,\theta) \\ \bar{\alpha}_3(x,\theta) \\ \bar{\alpha}_4(x,\theta) \\ \bar{\alpha}_5(x,\theta) \\ \bar{\alpha}_6(x,\theta) \\ \bar{\alpha}_7(x,\theta) \\ \bar{\alpha}_8(x,\theta) \end{pmatrix} = \begin{pmatrix} \alpha_1(x,\theta)/[-4x^2\sin\theta] \\ \alpha_2(x,\theta)/[2x^2\sin\theta] \\ \alpha_3(x,\theta)/[-2x^3\sin^2\theta] \\ \alpha_4(x,\theta)/[-3x^2\sin^2\theta] \\ \alpha_5(x,\theta)/[\sqrt{3}x^2\sin^2\theta] \\ \alpha_6(x,\theta)/[2x^2] \\ \alpha_7(x,\theta)/[2x^2] \\ \alpha_8(x,\theta)/[-2x^3\sin\theta] \end{pmatrix}, \tag{B1a}$$

$$\begin{pmatrix} \bar{\beta}_1(x,\theta) \\ \bar{\beta}_2(x,\theta) \\ \bar{\beta}_3(x,\theta) \end{pmatrix} = \begin{pmatrix} \beta_1(x,\theta)/[x] \\ \beta_2(x,\theta)/[-x^2\sin\theta] \\ \beta_3(x,\theta)/[-x\sin\theta] \end{pmatrix}. \tag{B1b}$$

These redefinitions rely on seven symmetry-axis boundary conditions, given by (3.6a), (3.6b), and (3.11b). The four remaining boundary conditions on the symmetry axis ($\bar{\theta} = 0,\ \pi$) are

$$\bar{\alpha}_6(x,\bar{\theta}) = 2\cos\theta\partial_\theta[\sin\theta\bar{\alpha}_1(x,\theta)]|_{\theta=\bar{\theta}}, \tag{B2a}$$

$$\bar{\alpha}_7(x,\bar{\theta}) = \cos\theta\partial_\theta[\sin\theta\bar{\alpha}_2(x,\theta)]|_{\theta=\bar{\theta}}, \tag{B2b}$$

$$\bar{\alpha}_8(x,\bar{\theta}) = \left(\cos^2\theta\bar{\alpha}_3 + \frac{1}{2}\sin\theta\cos\theta\partial_\theta\bar{\alpha}_3\right)\Big|_{\theta=\bar{\theta}}, \tag{B2c}$$

$$\partial_\theta\bar{\beta}_1(x,\theta)|_{\theta=\bar{\theta}} = 0. \tag{B2d}$$

The boundary conditions of the redefined *Ansatz* functions at spatial infinity take values in the range [0, 1],

$$\lim_{x\to 1}\begin{pmatrix} \bar{\alpha}_1(x,\theta) \\ \bar{\alpha}_2(x,\theta) \\ \bar{\alpha}_3(x,\theta) \\ \bar{\alpha}_4(x,\theta) \\ \bar{\alpha}_5(x,\theta) \\ \bar{\alpha}_6(x,\theta) \\ \bar{\alpha}_7(x,\theta) \\ \bar{\alpha}_8(x,\theta) \end{pmatrix} = \begin{pmatrix} (1+\sin^2\theta)/2 \\ \cos^2\theta \\ 1 \\ (1+2\sin^2\theta)/3 \\ 1 \\ 1 \\ 1 \\ 1 \end{pmatrix}, \tag{B3a}$$

$$\lim_{x\to 1}\begin{pmatrix} \bar{\beta}_1(x,\theta) \\ \bar{\beta}_2(x,\theta) \\ \bar{\beta}_3(x,\theta) \end{pmatrix} = \begin{pmatrix} \cos^2\theta \\ 1 \\ 1 \end{pmatrix}. \tag{B3b}$$

We now expand these redefined *Ansatz* functions, first in θ and then in x. Specifically, the θ expansion is given by

$$\begin{aligned} \bar{\alpha}_i(x,\theta) = {} & \frac{f_{i0}(x)}{2} \\ & + \sum_{n=1}^{N}[f_{in}(x)\cos(2n\theta) + p_{in}(x)\sin([2n-1]\theta)] \\ & + \begin{cases} p_{20}(x)|\cos\theta|, & \text{for } i=2, \\ p_{70}(x)/|\cos\theta|, & \text{for } i=7, \\ 0, & \text{for } i=1,3,4,5,6,8, \end{cases} \end{aligned} \tag{B4a}$$

$$\begin{aligned} \bar{\beta}_j(x,\theta) = {} & \frac{h_{j0}(x)}{2} \\ & + \sum_{n=1}^{N}[h_{jn}(x)\cos(2n\theta) + q_{jn}(x)\sin([2n-1]\theta)] \\ & + \begin{cases} q_{10}(x)|\cos\theta|, & \text{for } j=1, \\ 0, & \text{for } j=2,3. \end{cases} \end{aligned} \tag{B4b}$$

With the following boundary conditions at the origin:

$$f_{i0}(0) = 0, \quad \text{for } i = 2,7, \tag{B5a}$$

$$h_{10}(0) = 0, \tag{B5b}$$

$$f_{in}(0) = p_{in}(0) = h_{jn}(0) = q_{jn}(0) = 0, \quad \forall\, i,j \quad \text{and} \quad n > 0, \tag{B5c}$$

expansions (B4a) and (B4b) yield precisely the analytically determined behavior (4.1) near the origin, provided the radial functions $f(x)$, $h(x)$, $p(x)$ and $q(x)$ contain only positive powers of x. It can be seen, that consistency of the expansions (B4a) with the symmetry axis boundary conditions (B2) also demands that

$$p_{20}(x) = p_{70}(x), \tag{B6}$$

which we ensure by replacing p_{70} with p_{20} in the angular expansion.

The boundary conditions towards $x = 1$, given by (B3), require the following boundary conditions of our radial functions:

$$f_{\text{in}}(1) = \begin{pmatrix} +3/2 & 1 & 2 & +4/3 & 2 & 2 & 2 & 2 \\ -1/4 & 1/2 & 0 & -1/3 & 0 & 0 & 0 & 0 \end{pmatrix}, \quad \text{for } n \in [0,1], \tag{B7a}$$

$$h_{jn}(1) = \begin{pmatrix} 1 & 2 & 2 \\ 1/2 & 0 & 0 \end{pmatrix}, \quad \text{for } n \in [0,1], \tag{B7b}$$

$$f_{\text{in}}(1) = 0, \qquad h_{jn}(1) = 0, \quad \text{for } n > 1, \tag{B7c}$$

$$p_{\text{in}}(1) = 0, \quad q_{jn}(1) = 0, \quad \text{for } n \geq 0. \tag{B7d}$$

In addition, we must account for the four boundary conditions (B2) on the symmetry axis. We do this by fixing the radial profile functions f_{60}, f_{70}, f_{80} and q_{11} from the following conditions:

$$\frac{f_{60} - 2f_{10}}{2} + \sum_{n=1}^{N} [f_{6n} - 2f_{1n}] = 0, \tag{B8a}$$

$$\frac{f_{i,0} - f_{i-5,0}}{2} + \sum_{n=1}^{N} [f_{i,n} - f_{i-5,n}] = 0, \quad \text{for } i = 7,8, \tag{B8b}$$

$$\sum_{n=1}^{N} (2n-1) q_{1n} = 0. \tag{B8c}$$

We next expand the obtained radial functions in Legendre polynomials $P_m(2x-1)$ [these polynomials are normalized to $P_m(1) = 1$ and orthogonal over $x \in [0,1]$ with weight 1]:

$$f_{\text{in}}(x) = x^2 \sum_{m=0}^{M} a_{inm} P_m(2x-1) + \begin{cases} 2e_i, & \text{for } i = 1,3,4,5 \text{ and } n = 0, \\ 2e_{i-5}, & \text{for } i = 6,8 \text{ and } n = 0, \\ 0, & \text{for } i = 2,7 \text{ or } n > 0, \end{cases} \tag{B9a}$$

$$h_{jn}(x) = x^2 \sum_{m=0}^{M} b_{jnm} P_m(2x-1) + \begin{cases} 2e_{j+5}, & \text{for } j = 2,3, \text{ and } n = 0, \\ 0, & \text{for } j = 1 \text{ or } n > 0, \end{cases} \tag{B9b}$$

$$p_{\text{in}}(x) = x^2 \sum_{m=0}^{M} c_{inm} P_m(2x-1) + \begin{cases} e_2, & \text{for } i = 2 \text{ and } n = 0, \\ 0, & \text{for } n > 0, \end{cases} \tag{B9c}$$

$$q_{jn}(x) = x^2 \sum_{m=0}^{M} d_{jnm} P_m(2x-1) + \begin{cases} e_6, & \text{for } j = 1, \text{ and } n = 0, \\ 0, & \text{for } n > 0, \end{cases} \tag{B9d}$$

where the eight coefficients e_k are proportional to the eight origin coefficients from (4.1). The x^2 prefactors in (B9) ensure that the boundary conditions (B5) at the origin are always met, regardless of the values the expansion coefficients may take during the minimization process. Only the boundary conditions (B7) at $x = 1$ require fixing during minimization. This is easily done by adjusting one expansion coefficient of each radial function expansion in the following conditions:

$$\sum_{m=0}^{M} a_{inm} = f_{\text{in}}(1) - \begin{cases} 2e_i, & \text{for } i = 1,3,4,5 \text{ and } n = 0, \\ 2e_{i-5}, & \text{for } i = 6,8 \text{ and } n = 0, \\ 0, & \text{for } i = 2,7 \text{ or } n > 0, \end{cases} \tag{B10a}$$

$$\sum_{m=0}^{M} b_{jnm} = h_{jn}(1) - \begin{cases} 2e_{j+5}, & \text{for } j = 2,3, \text{ and } n = 0, \\ 0, & \text{for } j = 1 \text{ or } n > 0, \end{cases} \tag{B10b}$$

$$\sum_{m=0}^{M} c_{inm} = p_{\text{in}}(1) - \begin{cases} e_2, & \text{for } i = 2 \text{ and } n = 0, \\ 0, & \text{for } n > 0, \end{cases} \tag{B10c}$$

$$\sum_{m=0}^{M} d_{jnm} = q_{jn}(1) - \begin{cases} e_6, & \text{for } j = 1, \text{ and } n = 0, \\ 0, & \text{for } n > 0. \end{cases} \tag{B10d}$$

Cutting off both expansions at given N (for θ) and M (for x), we obtain a finite set of expansion coefficients over which we can minimize. Specifically, we minimize over all a_{imn} and b_{jmn} in the range $n \in [0, N]$, with the exception of a_{60m}, a_{70m} and a_{80m}, which are fixed by the symmetry axis conditions for all m. In addition, we minimize over all c_{imn} and d_{jmn} in the ranges $n \in [1, N]$ and $m \in [1, M]$, with the exception of d_{11m}, while the $m = 0$ coefficients are fixed by the boundary conditions at $x = 1$. Finally, we also minimize over the eight origin coefficients e_k and the

coefficients c_{20m} and d_{10m}. This, then, gives the following total number of coefficients:

$$N_{\text{coeff}}^{(\text{basic YMHth})} = 8 + [11(2N+1) - 2]M, \tag{B11}$$

which asymptotically goes as $22NM$ for N, $M \to \infty$.

APPENDIX C: NONCONTRACTIBLE SPHERE OF CONFIGURATIONS IN THE EXTENDED $SU(3)$ YMH THEORY

The basic idea behind the $\hat{S}$ construction has been sketched in Sec. III A. The relevant noncontractible sphere (NCS) of configurations is based on the $SU(3)$ matrix $U(\psi, \mu, \alpha, \theta, \phi)$ as given by Eqs. (3.1) and (3.2) of Ref. [3], where the coordinates (ψ, μ, α) parameterize the 3-sphere in configuration space and the coordinates (θ, ϕ) refer to 2-sphere at spatial infinity. The matrix at the "bottom" of the NCS $(\psi = 0)$ is given by

$$U(0, \mu, \alpha, \theta, \phi) = \begin{pmatrix} 1 & 0 & 0 \\ 0 & 0 & -1 \\ 0 & +1 & 0 \end{pmatrix} \equiv V, \tag{C1}$$

whereas the matrix at the "top" of the NCS $(\psi = \pi)$ is given by

$$U(\pi,\mu,\alpha,\theta,\phi) = \begin{pmatrix} \cos^2\theta & -\cos\theta\sin\theta e^{i\phi} & \sin\theta e^{-i\phi} \\ -\cos\theta\sin\theta e^{i\phi} & \sin^2\theta e^{2i\phi} & \cos\theta \\ -\sin\theta e^{-i\phi} & -\cos\theta & 0 \end{pmatrix} \equiv W(\theta,\phi). \tag{C2}$$

The field configurations of the NCS in the extended $SU(3)$ YMH theory have the same gauge fields as in Ref. [3],

$$gA_0(r,\theta,\phi)_{(\zeta)}^{(\text{NCS})} = 0, \tag{C3a}$$

$$gA_m(r,\theta,\phi)_{(\zeta)}^{(\text{NCS})} = -f(r)\partial_m U(\zeta,\theta,\phi)U^{-1}(\zeta,\theta,\phi), \tag{C3b}$$

and the following set of Higgs fields:

$$\Phi_1(r,\theta,\phi)_{(\zeta)}^{(\text{NCS})} = h_1(r)U(\zeta,\theta,\phi)\begin{pmatrix}\eta\\0\\0\end{pmatrix} + [1-h_1(r)]\cos^2\frac{\psi}{2}\begin{pmatrix}\eta\\0\\0\end{pmatrix}, \tag{C3c}$$

$$\begin{aligned}\Phi_2(r,\theta,\phi)_{(\zeta)}^{(\text{NCS})} &= h_2(r)U(\zeta,\theta,\phi)M_2\begin{pmatrix}\eta\\0\\0\end{pmatrix} + [1-h_2(r)]\cos^2\frac{\psi}{2}VM_2\begin{pmatrix}\eta\\0\\0\end{pmatrix} \\ &= h_2(r)U(\zeta,\theta,\phi)\begin{pmatrix}0\\0\\-\eta\end{pmatrix} + [1-h_2(r)]\cos^2\frac{\psi}{2}\begin{pmatrix}0\\\eta\\0\end{pmatrix},\end{aligned} \tag{C3d}$$

$$\begin{aligned}\Phi_3(r,\theta,\phi)_{(\zeta)}^{(\text{NCS})} &= h_3(r)U(\zeta,\theta,\phi)M_3^\dagger\begin{pmatrix}\eta\\0\\0\end{pmatrix} + [1-h_3(r)]\cos^2\frac{\psi}{2}VM_3^\dagger\begin{pmatrix}\eta\\0\\0\end{pmatrix} \\ &= h_3(r)U(\zeta,\theta,\phi)\begin{pmatrix}0\\\eta\\0\end{pmatrix} + [1-h_3(r)]\cos^2\frac{\psi}{2}\begin{pmatrix}0\\0\\\eta\end{pmatrix},\end{aligned} \tag{C3e}$$

with the short-hand notation $\zeta \equiv (\psi, \mu, \alpha)$ and the $SU(3)$ matrices M_2 and M_3 defined by (2.6). The radial functions $f(r)$ and $h_\alpha(r)$ of the NCS (C3) have boundary conditions

$$f(0) = h_1(0) = h_2(0) = h_3(0) = 0, \tag{C4a}$$

$$f(\infty) = h_1(\infty) = h_2(\infty) = h_3(\infty) = 1. \tag{C4b}$$

The NCS fields (C3) at $\psi = 0$, with $U = V$ from (C1), are given by

$$gA_0(r,\theta,\phi)^{(\text{NCS})}|_{\psi=0} = 0, \tag{C5a}$$

$$gA_m(r,\theta,\phi)^{(\text{NCS})}|_{\psi=0} = 0, \tag{C5b}$$

$$\Phi_1(r,\theta,\phi)^{(\text{NCS})}|_{\psi=0} = \begin{pmatrix}\eta\\0\\0\end{pmatrix}, \tag{C5c}$$

$$\Phi_2(r,\theta,\phi)^{(\mathrm{NCS})}|_{\psi=0} = \begin{pmatrix} 0 \\ \eta \\ 0 \end{pmatrix}, \tag{C5d}$$

$$\Phi_3(r,\theta,\phi)^{(\mathrm{NCS})}|_{\psi=0} = \begin{pmatrix} 0 \\ 0 \\ \eta \end{pmatrix}, \tag{C5e}$$

which correspond to the fields (2.9) of the classical vacuum.

For nontrivial radial functions $f(r)$ and $h_\alpha(r)$ with boundary conditions (C4), the NCS fields (C3) at $\psi = \pi$ correspond to a first approximation of the $\hat{S}$ fields in the extended theory. Specifically, these fields are given by

$$gA_0(r,\theta,\phi)^{(\mathrm{NCS})}|_{\psi=\pi} = 0, \tag{C6a}$$

$$gA_m(r,\theta,\phi)^{(\mathrm{NCS})}|_{\psi=\pi} = -f(r)\partial_m W(\theta,\phi)W^{-1}(\theta,\phi), \tag{C6b}$$

$$\Phi_1(r,\theta,\phi)^{(\mathrm{NCS})}|_{\psi=\pi} = h_1(r)W(\theta,\phi)\begin{pmatrix} \eta \\ 0 \\ 0 \end{pmatrix} = h_1(r)\eta\begin{pmatrix} \cos^2\theta \\ -\cos\theta\sin\theta e^{i\phi} \\ -\sin\theta e^{-i\phi} \end{pmatrix}, \tag{C6c}$$

$$\Phi_2(r,\theta,\phi)^{(\mathrm{NCS})}|_{\psi=\pi} = h_2(r)W(\theta,\phi)\begin{pmatrix} 0 \\ 0 \\ -\eta \end{pmatrix} = h_2(r)\eta\begin{pmatrix} -\sin\theta e^{-i\phi} \\ -\cos\theta \\ 0 \end{pmatrix}, \tag{C6d}$$

$$\Phi_3(r,\theta,\phi)^{(\mathrm{NCS})}|_{\psi=\pi} = h_3(r)W(\theta,\phi)\begin{pmatrix} 0 \\ \eta \\ 0 \end{pmatrix} = h_3(r)\eta\begin{pmatrix} -\cos\theta\sin\theta e^{i\phi} \\ \sin^2\theta e^{2i\phi} \\ -\cos\theta \end{pmatrix}, \tag{C6e}$$

in terms of the $SU(3)$ matrix W defined by (C2). As discussed in Sec. III A, the $\hat{S}$ *Ansatz* is obtained by a generalization of the fields (C6) and is presented in Sec. VI A.

APPENDIX D: $\hat{S}$ ENERGY DENSITY IN THE EXTENDED $SU(3)$ YMH THEORY

The $\hat{S}$ *Ansatz* in the extended $SU(3)$ Yang–Mills–Higgs theory (2.8) has been presented in Sec. VI A. The corresponding energy density is as follows:

$$\hat{e}(r,\theta)^{(\text{ext YMHth})} = \hat{e}_{\mathrm{YM}}(r,\theta) + \hat{e}_{\mathrm{Hkin},123}(r,\theta) + \hat{e}_{\mathrm{Hpot},123}(r,\theta), \tag{D1a}$$

$$\hat{e}_{\mathrm{Hkin},123}(r,\theta) = \hat{e}_{\mathrm{Hkin},1}(r,\theta) + \hat{e}_{\mathrm{Hkin},2}(r,\theta) + \hat{e}_{\mathrm{Hkin},3}(r,\theta), \tag{D1b}$$

where $\hat{e}_{\mathrm{YM}}$ equals the previous result (A1) and $\hat{e}_{\mathrm{Hkin},1}$ is identical to (A2). The Higgs fields Φ_2 and Φ_3 give the following further contributions:

$$\begin{aligned}\hat{e}_{\mathrm{Hkin},2}(r,\theta) = {}& \eta^2\{[\partial_r\beta_4]^2 + \cos^2\theta[\partial_r\beta_5]^2 + [\partial_r\beta_6]^2\} \\ & + \frac{\eta^2}{4r^2}\{[2\partial_\theta\beta_4 - \cos\theta\alpha_6\beta_5]^2 + [2\cos\theta\partial_\theta\beta_5 + \alpha_6\beta_4 - 2\sin\theta\beta_5]^2 \\ & + 4[\partial_\theta\beta_6]^2 + \cos^2\theta[\alpha_7\beta_4 + \alpha_8\beta_5]^2 + [\cos\theta\alpha_7\beta_6]^2 + [\alpha_8\beta_6]^2\} \\ & + \frac{\eta^2}{12r^2\sin^2\theta}\{[\sqrt{3}\cos^2\theta\alpha_1\beta_5 + 2\sqrt{3}\beta_4 + \sqrt{3}\alpha_4\beta_4 + \alpha_5\beta_4]^2 + 3[\alpha_2\beta_6]^2 \\ & + \cos^2\theta[\sqrt{3}(\alpha_1\beta_4 - \alpha_4\beta_5) + \alpha_5\beta_5]^2 + 3\cos^2\theta[\alpha_3\beta_6]^2 + 4[\alpha_5\beta_6]^2 + 3[\alpha_2\beta_4 + \cos^2\theta\alpha_3\beta_5]^2\},\end{aligned} \tag{D2a}$$

$$\hat{e}_{\mathrm{Hkin},3}(r,\theta) = \eta^2\{\cos^2\theta[\partial_r\beta_7]^2 + [\partial_r\beta_8]^2 + \cos^2\theta[\partial_r\beta_9]^2\} + \frac{\eta^2}{4r^2}\{[2\partial_\theta(\cos\theta\beta_7) - \alpha_6\beta_8 - \cos^2\theta\alpha_7\beta_9]^2 + [2\partial_\theta\beta_8 + \cos\theta\alpha_6\beta_7 - \cos\theta\alpha_8\beta_9]^2 + [2\partial_\theta(\cos\theta\beta_9) + \alpha_8\beta_8 + \cos^2\theta\alpha_7\beta_7]^2\} + \frac{\eta^2}{12r^2\sin^2\theta}\left\{\cos^2\theta[\sqrt{3}(\alpha_1\beta_8 + \alpha_2\beta_9) + \frac{\beta_7}{\sqrt{3}}(3\alpha_4 + \sqrt{3}\alpha_5 - 6)]^2 + [\cos^2\theta\sqrt{3}(\alpha_1\beta_7 + \alpha_3\beta_9) - \frac{\beta_8}{\sqrt{3}}(3\alpha_4 - \sqrt{3}\alpha_5 + 12)]^2 + \cos^2\theta[\sqrt{3}\alpha_2\beta_7 + \sqrt{3}\alpha_3\beta_8 - 2\alpha_5\beta_9]^2\right\}. \quad \text{(D2b)}$$

The potential energy density from the three Higgs triplets is given by

$$\hat{e}_{\mathrm{Hpot},123}(r,\theta) = \lambda\eta^4\{[\beta_1^2 + \cos^2\theta\beta_2^2 + \beta_3^2 - 1]^2 + [\beta_4^2 + \cos^2\theta\beta_5^2 + \beta_6^2 - 1]^2 + [\cos^2\theta\beta_7^2 + \beta_8^2 + \cos^2\theta\beta_9^2 - 1]^2 + [\beta_1\beta_4 + \cos^2\theta\beta_2\beta_5]^2 + [\beta_3\beta_6]^2 + \cos^2\theta[\beta_1\beta_7 + \beta_2\beta_8 + \beta_3\beta_9]^2 + \cos^2\theta[\beta_4\beta_7 + \beta_5\beta_8]^2 + \cos^2\theta[\beta_6\beta_9]^2\}. \quad \text{(D3)}$$

APPENDIX E: MINIMIZATION SETUP IN THE EXTENDED $SU(3)$ YMH THEORY

The numerical minimization procedure for $\hat{S}$ in the extended $SU(3)$ YMH theory (2.8) is similar to the one in the basic $SU(3)$ YMH theory (2.1). The procedure for the Yang-Mills *Ansatz* functions α_i $(i = 1, \ldots, 8)$ and the Higgs *Ansatz* functions β_k $(k = 1, 2, 3)$ remains unchanged. Their expansion coefficients and constraints are given in Appendix B.

In view of the behavior (6.5) at the origin and the boundary conditions (6.3b) towards spatial infinity, we redefine, by analogy with (B1), the further profile functions:

$$\begin{pmatrix} \bar{\beta}_4(x,\theta) \\ \bar{\beta}_5(x,\theta) \\ \bar{\beta}_6(x,\theta) \\ \bar{\beta}_7(x,\theta) \\ \bar{\beta}_8(x,\theta) \\ \bar{\beta}_9(x,\theta) \end{pmatrix} = \begin{pmatrix} \beta_4(x,\theta)/[-x\sin\theta] \\ \beta_5(x,\theta)/[-x] \\ \beta_6(x,\theta)/[x] \\ \beta_7(x,\theta)/[-x^2\sin\theta] \\ \beta_8(x,\theta)/[x^2\sin^2\theta] \\ \beta_9(x,\theta)/[-x] \end{pmatrix}. \quad \text{(E1)}$$

These redefinitions rely on three symmetry-axis boundary conditions, given by (6.4b) for $k = 4, 7$, and (6.4c) for $k = 8$. The three remaining boundary conditions on the symmetry axis $(\bar{\theta} = 0, \pi)$ are

$$\partial_\theta\bar{\beta}_k(x,\theta)|_{\theta=\bar{\theta}} = 0 \quad \text{for } k = 5, 6, 9. \quad \text{(E2)}$$

The boundary conditions of the redefined *Ansatz* functions at spatial infinity are then

$$\lim_{x\to 1}\begin{pmatrix} \bar{\beta}_4(x,\theta) \\ \bar{\beta}_5(x,\theta) \\ \bar{\beta}_6(x,\theta) \\ \bar{\beta}_7(x,\theta) \\ \bar{\beta}_8(x,\theta) \\ \bar{\beta}_9(x,\theta) \end{pmatrix} = \begin{pmatrix} 1 \\ 1 \\ 0 \\ 1 \\ 1 \\ 1 \end{pmatrix}. \quad \text{(E3)}$$

Almost identical to (B4b), we define the following angular expansions of the redefined *Ansatz* functions:

$$\bar{\beta}_k(x,\theta) = \frac{h_{k0}(x)}{2} + \sum_{n=1}^{N}[h_{kn}(x)\cos(2n\theta) + q_{kn}(x)\sin([2n-1]\theta)] + \begin{cases} q_{60}(x)|\cos\theta|, & \text{for } k = 6, \\ 0, & \text{for } k = 4, 5, 7, 8, 9, \end{cases} \quad \text{(E4)}$$

with the following boundary conditions at the origin:

$$h_{60}(0) = 0, \quad \text{(E5a)}$$

$$h_{kn}(0) = q_{kn}(0) = 0, \quad \forall\, i, k \quad \text{and} \quad n > 0. \quad \text{(E5b)}$$

With these constraints, the profile functions behave as (6.5) near the origin. The boundary conditions at $x = 1$ translate to those of the radial functions $h(x)$ and $q(x)$,

$$h_{kn}(1) = \begin{pmatrix} 2 & 2 & 0 & 2 & 2 & 2 \\ 0 & 0 & 0 & 0 & 0 & 0 \end{pmatrix}, \quad \text{for } k = 4, \ldots, 9 \quad \text{and} \quad n \in [0, 1], \quad \text{(E6a)}$$

$$h_{kn}(1) = 0, \quad \text{for } n > 1, \tag{E6b}$$

$$q_{kn}(1) = 0, \quad \text{for } n \geq 0. \tag{E6c}$$

The three boundary conditions (E2) on the symmetry axis are implemented by fixing the radial profile functions q_{51}, q_{61} and q_{91} from the following equations:

$$\sum_{n=1}^{N} (2n-1) q_{kn} = 0, \quad \text{for } k = 5, 6, 9. \tag{E7}$$

We next expand the radial functions in Legendre polynomials $P_m(2x-1)$,

$$h_{kn}(x) = x^2 \sum_{m=0}^{M} b_{knm} P_m(2x-1) + \begin{cases} 2e_{k+5}, & \text{for } k = 4,5,7,8,9 \quad \text{and} \quad n = 0, \\ 0, & \text{for } k = 6 \quad \text{or} \quad n > 0, \end{cases} \tag{E8a}$$

$$q_{kn}(x) = x^2 \sum_{m=0}^{M} d_{knm} P_m(2x-1) + \begin{cases} e_{11}, & \text{for } k = 6 \quad \text{and} \quad n = 0, \\ 0, & \text{for } n > 0, \end{cases} \tag{E8b}$$

with x^2 prefactors to ensure that the correct origin behavior is reproduced. We enforce the boundary conditions (E6) at $x = 1$ by adjusting one expansion coefficient of each radial function expansion in the following conditions:

$$\sum_{m=0}^{M} b_{knm} = h_{kn}(1) - \begin{cases} 2e_{k+5}, & \text{for } k = 4,5,7,8,9 \quad \text{and} \quad n = 0, \\ 0, & \text{for } k = 6 \quad \text{or} \quad n > 0, \end{cases} \tag{E9a}$$

$$\sum_{m=0}^{M} d_{knm} = q_{kn}(1) - \begin{cases} e_{11}, & \text{for } k = 6 \quad \text{and} \quad n = 0, \\ 0, & \text{for } n > 0. \end{cases} \tag{E9b}$$

The total number of coefficients for given radial (M) and angular (N) expansion cut-offs is given by

$$N_{\text{coeff}}^{(\text{ext YMHth})} = 14 + [17(2N+1) - 5]M, \tag{E10}$$

which asymptotically goes as $34NM$ for $N, M \to \infty$.

[1] W. A. Bardeen, Anomalous Ward identities in spinor field theories, Phys. Rev. **184**, 1848 (1969).
[2] F. R. Klinkhamer, Z–string global gauge anomaly and Lorentz non-invariance, Nucl. Phys. **B535**, 233 (1998).
[3] F. R. Klinkhamer and C. Rupp, A new sphaleron for the non-Abelian anomaly, Nucl. Phys. **B709**, 171 (2005).
[4] F. R. Klinkhamer and N. S. Manton, A saddle point solution in the Weinberg-Salam theory, Phys. Rev. D **30**, 2212 (1984).
[5] F. R. Klinkhamer and R. Laterveer, The sphaleron at finite mixing angle, Z. Phys. C **53**, 247 (1992).
[6] J. Kunz, B. Kleihaus, and Y. Brihaye, Sphalerons at finite mixing angle, Phys. Rev. D **46**, 3587 (1992).
[7] S. Weinberg, Mixing angle in renormalizable theories of weak and electromagnetic interactions, Phys. Rev. D **5**, 1962 (1972).
[8] C. Patrignani *et al.* (Particle Data Group Collaboration), The review of particle physics (2016), Chin. Phys. C **40**, 100001 (2016).
[9] F. R. Klinkhamer, Construction of a new electroweak sphaleron, Nucl. Phys. **B410**, 343 (1993).
[10] F. R. Klinkhamer and C. Rupp, Sphalerons, spectral flow, and anomalies, J. Math. Phys. (N.Y.) **44**, 3619 (2003).
[11] M. Haberichter, Untersuchungen des $SU(3)$ Sphalerons, Diplomarbeit, Universität Karlsruhe (TH), 2009.
[12] M. Schuh, Weitere Untersuchungen des $SU(3)$ Sphalerons $\hat{S}$, Diplomarbeit, Karlsruhe Institute of Technology, 2014.
[13] P. Nagel, Energy and structure analysis of the $SU(3)$ sphaleron, Diplomarbeit, Karlsruhe Institute of Technology, 2014.
[14] S. Kirkpatrick, C. D. Gelatt, and M. P. Vecchi, Optimization by simulated annealing, Science **220**, 671 (1983).
[15] D. Kraft, A software package for sequential quadratic programming, Technical Report DFVLR-FB 88-28, Institut fur Dynamik der Flugsysteme, Oberpfaffenhofen, Germany, 1988.
[16] E. Jones, T. Oliphant, P. Peterson *et al.*, SciPy: Open source scientific tools for Python, 2001, http://www.scipy.org/.
[17] G. 't Hooft, A planar diagram theory for strong interactions, Nucl. Phys. **B72**, 461 (1974).
[18] T. H. R. Skyrme, A nonlinear field theory, Proc. R. Soc. A **260**, 127 (1961).
[19] E. Witten, Baryons in the $1/N$ expansion, Nucl. Phys. **B160**, 57 (1979).
[20] E. Witten, Current algebra, baryons, and quark confinement, Nucl. Phys. **B223**, 433 (1983).